

1 A New Operational Mediterranean Diurnal Optimally Interpolated

2 SST Product within the Copernicus Marine Environment

3 Monitoring Service

4 Andrea Pisano¹, Daniele Ciani¹, Salvatore Marullo^{1,2} Rosalia Santoleri¹, Bruno Buongiorno Nardelli³

5 ¹CNR-ISMAR, Via del Fosso del Cavaliere 100, Rome, 00133, Rome, Italy

6 ²ENEA, Via Enrico Fermi, 45, 00044 Frascati, Italy

7 ³CNR-ISMAR, Calata Porta di Massa, Napoli, 80133, Italy

8
9 *Correspondence to:* Andrea Pisano (andrea.pisano@cnr.it)

10 **Abstract.** Within the Copernicus Marine Environment Monitoring Service (CMEMS), a new operational MEDiterranean
11 Diurnal Optimally Interpolated [Sea Surface Temperature](#) (MED DOISST) product has been developed. This product provides
12 hourly mean maps (Level-4) of sub-skin SST at 1/16° horizontal resolution over the Mediterranean Sea from January 2019 to
13 present. [Sub-skin is the temperature at ~1 mm depth of the ocean surface, and then potentially subject to a large diurnal cycle.](#)
14 The product is built by combining hourly SST data from the Spinning Enhanced Visible and InfraRed Imager (SEVIRI) on
15 board Meteosat Second Generation and model analyses through optimal interpolation. SEVIRI and model data are respectively
16 used as the observation source and first-guess. [The choice of using a model output as first-guess represents an innovative
17 alternative to the commonly adopted climatologies or previous analyses, providing physically consistent estimates of hourly
18 SSTs in the absence of any observation or in situ measurement.](#)The differences between satellite and model SST are free, or
19 nearly free, of any diurnal cycle, thus allowing them to be interpolated in space and time using satellite data acquired at
20 [different times of the day.](#) The accuracy of the MED DOISST product is assessed here by comparison against surface drifting
21 buoy measurements, covering the years 2019 and 2020. The diurnal cycle reconstructed from DOISST is in good agreement
22 with the one observed by independent drifter data, with a mean bias of 0.041 ± 0.001 K and root-mean-square difference
23 (RMSD) of 0.412 ± 0.001 K. The new SST product is more accurate than the input model during the central warming hours,
24 when the model, on average, underestimates drifter SST by one tenth of degree. [The capability of DOISST to reconstruct
25 diurnal warming events, which may reach intense amplitudes larger than 5 K in the Mediterranean Sea, is also analysed.
26 Specifically, a comparison with the OSTIA diurnal skin SST product, SEVIRI, model and drifter data, shows that the DOISST
27 product is able to reproduce more accurately diurnal warming events larger than 1 K.](#)The MED-DOISST product is also able
28 to reproduce accurately the extreme diurnal warming events frequently observed in the Mediterranean Sea, which may reach
29 [amplitudes larger than 5 K during the warm season.](#) This product can contribute to improve the prediction capability of

numerical weather forecast systems (e.g., through improved forcing/assimilation), as well as the monitoring of surface heat budget estimates and temperature extremes which can have significant impacts on the marine ecosystem.

The full MED DOISST product (released on 04 May 2021) is available upon free registration at https://doi.org/10.25423/CMCC/SST_MED_PHY_SUBSKIN_L4_NRT_010_036 (Pisano et al., 2021). The reduced subset used here for validation and review purposes is openly available at <https://doi.org/10.5281/zenodo.5807729> (Pisano, 2021).

1 Introduction

In the last decades, the development of accurate satellite-based Sea Surface Temperature (SST) products required an increasing effort to meet an ever-growing request from scientific, operational and emerging policy needs. Indeed, infrared and/or microwave satellite radiometers allow a systematic and synoptic mapping of the ocean surface temperature (under clear-sky conditions for the infrared and in the absence of rain for the microwave bands) with spatial resolutions from one to few kilometers and temporal sampling from hourly to daily (Minnett et al., 2019). This almost continuous coverage represents a unique characteristic of satellite thermal data, which is clearly not achievable with the use of in situ measurements alone. Indeed, though in situ sensors reach significantly higher accuracy than satellite sensors, with uncertainties that can reach $O(10^{-2} \text{ K}^{\circ}\text{E})$, they provide pointwise seawater temperature measurements, generally characterized by a poor and non-uniform sampling of the ocean surface.

There is a huge variety of satellite-based SST datasets, characterized by different nominal resolutions as well as temporal and spatial (global or regional) coverage, and based on different processing algorithms and satellite sensors, but designed to provide highly accurate SST estimates (Yang et al., 2021). Operational datasets are typically distributed in near real time (NRT), delayed-mode or as reprocessed datasets, and may include different processing levels, from single satellite passes processed to provide valid SST values in the original observation geometry, the so-called Level-2 (L2), to images remapped onto a regular grid, also known as Level-3 (L3), up to the spatially complete Level-4 (L4), interpolated over fixed regular grids. These latter are required by several applications since the lower levels are typically affected by several data voids (due to clouds, rain, land, sea-ice, or other environmental factors depending on the type of sensors). The timely availability of SST data, ranging from a few hours to a few days before real time, allows their use as boundary condition and/or assimilation in meteorological and ocean forecasting systems (Waters et al., 2015), to improve the retrieval of ocean surface currents (Bowen et al., 2002; Rio and Santoleri 2018), and monitor some weather extreme events, such as marine heatwaves (Oliver et al., 2021). The reprocessing of long-term SST data records, typically covering the satellite era (1981-present), aims to provide more stable and consistent datasets, complementing the NRT production, to be used to investigate climate variability and monitor changes from interannual to multi-decadal timescales (Deser et al., 2010), including e.g. SST trends' estimates (Good et al., 2007;

61 Pisano et al., 2020). The Copernicus Marine Environment Monitoring Service (CMEMS) is one of the main examples of how
62 satellite observations, including not only SST but a wide range of surface variables (e.g., sea surface salinity, sea surface
63 height, ocean color, winds and waves), are exploited to derive and disseminate high-level products (Le Traon et al., 2019),
64 namely L4 data in order to be directly usable for downstream applications.

65 The majority of the existing L4 SST datasets are provided as daily, weekly or monthly averaged fields (see e.g. Fiedler et al.,
66 2019; Yang et al., 2021). Examples of well-known state-of-the-art SST daily datasets include the Global Ocean Sea Surface
67 Temperature and Sea Ice (OSTIA) dataset (Good et al., 2020), the European Space Agency (ESA) Climate Change Initiative
68 (CCI), the Copernicus Climate Change Service (C3S) Reprocessed Sea Surface Temperature Analyses (Merchant et al., 2019),
69 and the NOAA Daily Optimally Interpolated SST (OISST) v2.1 dataset, previously known/referred to as Reynolds SST
70 analysis (Huang et al., 2021). Though a daily resolution is generally sufficient to meet the requirements of many of the
71 oceanographic applications, it does not resolve the SST diurnal cycle, the typical day-night SST oscillation mainly driven by
72 solar heating. Within the oceanic thermal skin layer (few μm to 1 mm), SST is typically subject to a large potential diurnal
73 cycle (especially under low wind speed and strong solar heating conditions) reaching amplitudes up to 3 K in the world oceans
74 (Gentemann et al., 2008; Gentemann and Minnett, 2008).

75 The SST diurnal cycle has several implications on mixed layer dynamics, air-sea interaction and the modulation of the lower
76 atmosphere dynamics. The most direct consequence of the SST diurnal amplitude variability is certainly on air-sea fluxes.
77 Clayson and Bogdanoff (2013) estimated that the diurnal SST cycle contributes ~~with slightly less than that~~ approximately 5
78 Wm^{-2} to the global ocean-atmosphere heat budget with peaks of about 10 Wm^{-2} in the Tropics. The inclusion of a realistic
79 diurnal SST cycle in atmospheric numerical simulation also has a non-negligible impact on cloud dynamics. Chen and Houze
80 (1997) have shown that in the Tropical Warm Pool, where extreme localized warming events occur, the diurnal warming can
81 contribute to modulate the evolution of convective clouds and, more in general, can impact the ocean-atmosphere coupling in
82 numerical models, producing a more realistic spatial pattern of warming and precipitation (Bernie et al., 2008). Overall, the
83 diurnal cycle of SST is generally underestimated in current ocean models and the assimilation of SST at high temporal
84 frequency has the potential to improve sea surface variability and mixed layer accuracy (Storto and Oddo, 2019).

85 In principle, the best opportunity to measure the diurnal cycle comes from infrared radiometers on board geostationary
86 satellites. Their observations are sufficiently accurate and frequent to resolve the diurnal signal variability whenever cloud
87 cover is not too persistent. An example is provided by the Spinning Enhanced Visible Infra-Red Imager (SEVIRI) onboard the
88 Meteosat Second Generation (MSG) geostationary satellite covers. The operational retrieval of SST from MSG/SEVIRI
89 (managed by the European Organization for the Exploitation of Meteorological Satellites, EUMETSAT, Ocean and Sea-Ice
90 Facility, OSI-SAF) produces L3C hourly sub-skin SST products by aggregating 15 minutes (MSG/SEVIRI) observations
91 within 1 hour. The sub-skin SST is the temperature at the base of the conductive laminar sub-layer of the ocean surface, as
92 defined by the Group of High Resolution SST (GHRSSST, see e.g. Minnett et al., 2019). In practice, this is the temperature at

93 ~1 mm depth (see e.g., [osisaf_cdop3_ss1_pum_msg_sst_data_record.pdf \(eumetsat.int\)](#)), and thus particularly sensitive to
94 diurnal warming.

95 For the global ocean, the Operational Sea surface Temperature and sea Ice Analysis (OSTIA) diurnal product (While et al.,
96 2017) provides daily gap-free maps of hourly mean skin SST at $0.25^\circ \times 0.25^\circ$ horizontal nominal resolution, using in situ and
97 satellite data from infrared radiometers. [The skin temperature is defined as the temperature of the ocean measured by an
98 infrared radiometer \(typically aboard satellites\) and represents the temperature of the ocean within the conductive diffusion-
99 dominated sub-layer at a depth of ~10-20 \$\mu\text{m}\$](#) ~~The skin SST is the temperature within the conductive diffusion-dominated sub-
100 layer at a depth of ~10-20 μm (as defined by GHRSSST, Minnett et al., 2019).~~ This system produces a skin SST by combining
101 the OSTIA foundation SST analysis (Good et al., 2020) with a diurnal warm-layer temperature difference and a cool skin
102 temperature difference derived from numerical models.

103 At regional scale, a method to reconstruct the hourly SST field over the Mediterranean Sea from SEVIRI data has been
104 proposed by Marullo et al. (2014, 2016). The reconstruction is based on a blending of satellite observations and numerical
105 model analyses (used as first-guess) using optimal interpolation. Though model analyses by definition also assimilate
106 observations, which could thus in principle include hourly SEVIRI data, in the present configuration they are not able to deal
107 with such frequent updates (see section 2.2), and the approach presented here represents an effective way to improve the
108 reconstruction of SST daily cycle from high-repetition satellite measurements. Previous works demonstrated the capability of
109 SEVIRI to resolve the SST diurnal variability and to reconstruct accurate L4 SST hourly fields over the Mediterranean Sea, a
110 basin that exhibits large diurnal SST variations (Buongiorno Nardelli et al., 2005; Minnett et al., 2019) that can easily exceed
111 extreme values (~5 K) as observed in the Tropical Pacific (Chen and Houze 1997), in the Atlantic Ocean and other marginal
112 seas (Gentemann et al., 2008; Merchant et al., 2008). The aim of this paper is to describe the operational implementation of a
113 diurnal optimally interpolated SST (DOISST) product for the Mediterranean Sea (MED) ~~at $1/16^\circ$ horizontal resolution,~~
114 building on the algorithm by Marullo et al. (2014, 2016). [The DOISST product routinely provides hourly mean maps of sub-
115 skin SST at \$1/16^\circ\$ horizontal resolution over the Mediterranean Sea from January 2019 to present.](#) The assessment [presented
116 here for of](#) the MED-DOISST product covers two complete years (2019-2020), thus extending previous similar validations
117 (Marullo et al., 2016).

119 2 The data

120 2.1 Satellite data

121 Input satellite SST is derived from the SEVIRI sensor onboard the Meteosat Second Generation (Meteosat-11) satellite.
122 SEVIRI has a repeat cycle of 15 minutes over the 60S-60N and 60W-60E domain: Atlantic Ocean, European Seas and western

123 Indian Ocean. The retrieval of SST from Meteosat-11/SEVIRI is managed by EUMETSAT OSI-SAF, which provides sub-
124 skin SST data as aggregated (L3C) hourly products remapped onto a 0.05° regular grid. Hourly products result from
125 compositing the best SST measurements available in one hour and are made available in near real time with a timeliness of 3
126 hours (see the OSI-SAF product user manual, <https://osi-saf.eumetsat.int/products/osi-206>). File format follows the Data
127 Specification (GDS) version 2 from the Group for High Resolution Sea Surface Temperatures (GHRSSST, [https://podaac-
128 tools.jpl.nasa.gov/drive/files/OceanTemperature/ghrsst/docs/GDS20r5.pdf](https://podaac-tools.jpl.nasa.gov/drive/files/OceanTemperature/ghrsst/docs/GDS20r5.pdf)). The computation of SST in day and night
129 conditions is based on a nonlinear split window algorithm whose coefficients are determined from brightness temperature
130 simulations on a radiosonde profile database, with an offset coefficient corrected relative to buoy measurements. A correction
131 term derived from simulated brightness temperatures with an atmospheric radiative transfer model is then applied to the
132 multispectral derived SST (OSI-SAF PUM, https://osi-saf.eumetsat.int/lml/doc/osisaf_cdop3_ss1_pum_geo_sst.pdf). L3C
133 data are provided with additional information, including quality level and cloud flags. Such quality flags are provided at pixel
134 level, ranging over a scale of five levels with increasing reliability: 1 (“cloudy”), 2 (“bad”), 3 (“acceptable”), 4 (“good”) to 5 (“excellent”).
135

136 The accuracy of Meteosat-11 SST data has been assessed through comparison with co-located drifting buoys, for day and
137 night data separately covering the period from February to June 2018 (see the OSI-SAF scientific validation report, [https://osi-
138 saf.eumetsat.int/lml/doc/osisaf_cdop2_ss1_geo_sst_val_rep.pdf](https://osi-saf.eumetsat.int/lml/doc/osisaf_cdop2_ss1_geo_sst_val_rep.pdf)). The mean bias and standard deviation (derived from the
139 differences between SEVIRI SSTs and drifter measurements over a matchup database) during nighttime have been quantified
140 in -0.1 K and 0.53 K, respectively. During daytime, the bias remains practically unchanged (-0.09 K) and the standard deviation
141 slightly higher (0.56 K). These statistics were derived by selecting SEVIRI SST with quality flags ≥ 3 , and it is shown that the
142 quality of SST improves when choosing higher quality levels. [A similar validation procedure \(Marullo et al., 2016\), but
143 performed over the Mediterranean Sea by using nighttime and daytime data selected with quality flags \$\geq 4\$, shows that SEVIRI
144 SST bias and standard deviation are -0.03 K and 0.47 K, respectively.](#)

145 For our purposes, we selected L3C SST data with quality flag ≥ 3 , as also indicated/suggested in the OSI-SAF scientific
146 validation report. [A synthesis of the SEVIRI SST characteristics is reported in Table 1.](#)

147 **2.2 Model data**

148 The model output fields of surface temperature are derived from the CMEMS Mediterranean Sea Physical Analysis and
149 Forecasting product, and identified as MEDSEA_ANALYSIS_FORECAST_PHY_006_013
150 ([https://resources.marine.copernicus.eu/product-
151 detail/MEDSEA_ANALYSISFORECAST_PHY_006_013/INFORMATION](https://resources.marine.copernicus.eu/product-detail/MEDSEA_ANALYSISFORECAST_PHY_006_013/INFORMATION);
152 https://doi.org/10.25423/CMCC/MEDSEA_ANALYSISFORECAST_PHY_006_013_EAS6; last access: 03 November 2021;
153 Clementi et al., 2021), and routinely produced by the CMEMS Mediterranean Monitoring and Forecasting Center (Med-MFC).
154 The modelling system is based on the Mediterranean Forecasting System, MFS (Pinardi et al., 2003), a coupled hydrodynamic-

155 wave model implemented over the Mediterranean basin, extended into the Atlantic Sea in order to better resolve the exchanges
156 with the Atlantic Ocean at the Strait of Gibraltar, with a horizontal grid resolution of $1/24^\circ$ (~4 km) and 141 unevenly spaced
157 vertical levels (Clementi et al., 2017). The Ocean General Circulation Model is based on the Nucleus for European Modelling
158 of the Ocean (NEMO v3.6) (Oddo et al., 2014, 2009), while the wave component is provided by Wave Watch-III. The model
159 solutions are corrected by a variational data assimilation scheme (3DVAR) of temperature and salinity vertical profiles and
160 along track satellite sea level anomaly observations (Dobricic and Pinardi 2008). The CMEMS Mediterranean SST L4 product
161 (CMEMS product reference: SST_MED_SST_L4_NRT_OBSERVATIONS_010_004,
162 [https://resources.marine.copernicus.eu/product-
163 detail/SST_MED_SST_L4_NRT_OBSERVATIONS_010_004/INFORMATION](https://resources.marine.copernicus.eu/product-detail/SST_MED_SST_L4_NRT_OBSERVATIONS_010_004/INFORMATION); last access: 03 November 2021) is used for
164 the correction of surface heat fluxes with the relaxation constant of $110 \text{ Wm}^{-2}\text{K}^{-1}$ centered at midnight since the product
165 provides foundation SST (~SST at midnight).

166 The Med-MFC product is produced with two different cycles: a daily cycle for the production of forecasts (i.e., ten-days
167 forecast on a daily basis), and a weekly cycle for the production of analyses. For our purposes, only hourly mean fields of sea
168 surface temperature, which correspond to the first vertical level of the model centered at ~1 m from the surface, are selected.
169 [A synthesis of the model-derived SST characteristics is reported in Table 1.](#)

170 2.3 In situ data

171 ~~[Surface drifting buoys have been used for validation purposes \(Section 4\). Since there are no in situ instruments able to](#)~~
172 ~~[routinely measure skin/sub-skin SSTs, the commonly adopted validation procedure is to use drifters' data, also due to their](#)~~
173 ~~[high accuracy and closeness to the sea surface \(their representative depth attains around ~20 cm; Reverdin et al., 2010\), and](#)~~
174 ~~[to their abundance compared to other in situ instruments, which allows to achieve a more consistent and homogeneous temporal](#)~~
175 ~~[and spatial coverage. Of course, these observations are affected by a representativeness error when compared to sub-skin SSTs,](#)~~
176 ~~[which is typically quantified in terms of a bias between the two estimates. In situ data have been used for validation purposes](#)~~
177 ~~[\(Section 4\). Specifically, only surface drifting buoys have been used due to both their closeness to the sea surface \(typically](#)~~
178 ~~[~20 cm from the surface; Reverdin et al., 2010\) and to their much larger number compared to other in situ instruments, which](#)~~
179 ~~[allows a more consistent and homogeneous temporal and spatial coverage.](#)~~

180 Drifter data have been obtained from the CMEMS IN SITU (INS) TAC (identified as
181 INSITU_MED_NRT_OBSERVATIONS_013_035, [https://resources.marine.copernicus.eu/product-
182 detail/INSITU_MED_NRT_OBSERVATIONS_013_035/INFORMATION](https://resources.marine.copernicus.eu/product-detail/INSITU_MED_NRT_OBSERVATIONS_013_035/INFORMATION); and
183 INSITU_IBI_NRT_OBSERVATIONS_013_033, [https://resources.marine.copernicus.eu/product-
184 detail/INSITU_IBI_NRT_OBSERVATIONS_013_033/INFORMATION](https://resources.marine.copernicus.eu/product-detail/INSITU_IBI_NRT_OBSERVATIONS_013_033/INFORMATION); last access: 03 November 2021), which collects
185 and distributes a variety of physical and biogeochemical seawater measurements, provided with the same homogeneous file
186 format. Each in situ measurement, including drifters, undergoes automated quality controls before its distribution. The quality

187 of the data is expressed by control flags indexed from 0 to 9, with the value of 1 indicating best quality. Drifter data have been
188 used to compile an hourly matchup database of co-located (in space and time) diurnal optimally interpolated SST (DOISST)
189 values and model outputs (Section 4.1), and validation statistics are based on the comparison ~~between-among~~ DOISST, model
190 SST and drifting buoy measurements over the matchup database (Section 4.2). A synthesis of the drifter SST characteristics is
191 reported in Table 1.

192 **2.4 OSTIA diurnal**

193 The OSTIA diurnal skin SST product (While et al., 2017) provides gap-free global maps of hourly mean skin SST at 0.25° x
194 0.25° horizontal resolution, obtained by combining in situ and infrared satellite data. This product is operationally produced
195 by the Met Office within the Copernicus Marine Service (identified as
196 SST_GLO_SST_L4_NRT_OBSERVATIONS_010_014, [https://resources.marine.copernicus.eu/product-](https://resources.marine.copernicus.eu/product-detail/SST_GLO_SST_L4_NRT_OBSERVATIONS_010_014/INFORMATION)
197 detail/SST_GLO_SST_L4_NRT_OBSERVATIONS_010_014/INFORMATION; last access: 02 May 2022), and created
198 using the Operational Sea surface Temperature and Ice Analysis (OSTIA) system (Good et al., 2020). The OSTIA system also
199 produces a global daily average foundation SST L4 product (identified as
200 SST_GLO_SST_L4_NRT_OBSERVATIONS_010_001, [https://resources.marine.copernicus.eu/product-](https://resources.marine.copernicus.eu/product-detail/SST_GLO_SST_L4_NRT_OBSERVATIONS_010_001/INFORMATION)
201 detail/SST_GLO_SST_L4_NRT_OBSERVATIONS_010_001/INFORMATION; last access: 02 May 2022). Since the skin
202 SST can be considered as the sum of three components, namely the foundation SST, the warm layer and the cool skin, the
203 OSTIA diurnal product is created by adjusting the OSTIA foundation SST analysis with a modelled diurnal warm layer analysis
204 (which assimilates satellite observations) and a cool skin model, based respectively on the Takaya (Takaya et al., 2010) and
205 Artale models (Artale et al., 2002). Assimilation into the warm layer model makes use of SEVIRI, GOES-W and MTSAT-2
206 geostationary infrared sensors, and of the polar orbiting VIIRS radiometer. Further details on the method can also be found in
207 Copernicus PUM (<https://catalogue.marine.copernicus.eu/documents/PUM/CMEMS-SST-PUM-010-014.pdf>). A synthesis of
208 the OSTIA diurnal SST characteristics is reported in Table 1.

SST							
Source	Definition	Vertical level	Spatial res.	Temporal res.	Spatial coverage	Temporal coverage	Processing level
Model	Depth SST	1 m (first model layer)	0.042°x0.042°	Hourly	17.3°W–36.3°E, 30.2°N–46°N	2019-Present	Model output
SEVIRI	Sub-skin SST	~1 mm (surface only)	0.05°x0.05°	Hourly	60°W–60°E, 60°S–60°N	2015-Present	L3C
OSTIA diurnal	Skin SST	~10-20 μm (surface only)	0.25°x0.25°	Hourly	Global	2015-Present	L4
Surface Drifting Buoys	Depth SST	~20 cm (surface only)	Not applicable	Hourly	30°W–36.5°E, 20°N–55°N	2010-Present	L2

Tabella formattata

Table 1. Summary of the SST products used to produce (Model and SEVIRI), validate (surface drifting buoys), and intercompare (all) the DOISST product. The SST nomenclature (skin, sub-skin, and depth) follows the Group for High Resolution Sea Surface Temperatures (GHRSSST) definitions (<https://podaac-tools.jpl.nasa.gov/drive/files/OceanTemperature/ghrssst/docs/GDS20r5.pdf>).

Formattato: Tipo di carattere: Grassetto

3 The Mediterranean diurnal optimally interpolated SST product

3.1 Product overview

The Mediterranean diurnal optimally interpolated SST (hereafter referred to as MED DOISST) operational product consists of hourly mean gap-free (L4) satellite-based estimates of the sub-skin SST over the Mediterranean Sea (plus the adjacent Eastern Atlantic box, see Section 2.2) at 0.0625° x 0.0625° grid resolution, from 1st January 2019 to near real time. Specifically, the product is updated daily and provides 24 hourly mean data of the previous day, centered at 00:00, 01:00, 02:00, ..., 23:00 UTC. The MED DOISST product is published on the CMEMS on line catalogue and identified as SST_MED_PHY_SUBSKIN_L4_NRT_010_036 (CMEMS product reference) and cmems_obs-sst_med_phy-sst_nrt_diurnal-oi-0.0625deg_PT1H-m (CMEMS dataset reference). Further details on the product characteristics are provided in Table 2. A synthesis of the product characteristics is shown Table 1.

DOISST is the result of a blending of sub-skin SSTs and modelled SSTs (as detailed in the next section), the former representative of a depth of 1 mm and the latter of 1 m. Then, the DOISST effective depth does, in principle, vary between 1 mm up to 1 m, depending on how many satellite observations enter the interpolation. As diurnal warming is significantly reduced under cloudy conditions, however, the difference between the SST at 1 m and the sub-skin SST will be much smaller

when SEVIRI observations are not present. For this reason, we can define the DOISST product as representative of sub-skin values.

CMEMS Product ID: SST_MED_PHY_SUBSKIN_L4_NRT_010_036

CMEMS Dataset ID: cmems_obs-sst_med_phy-sst_nrt_diurnal-oi-0.0625deg_PT1H-m

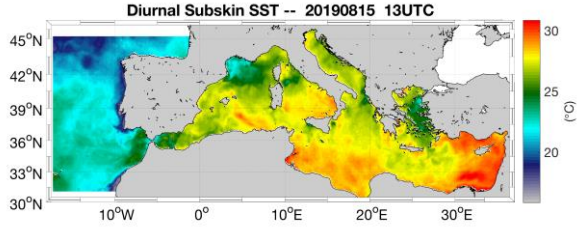
General description	<p>The CMEMS Mediterranean diurnal product provides near-real-time, hourly mean, gap-free (L4) sub-skin SST fields over the Mediterranean Sea and the adjacent Atlantic box over a 0.0625°x0.0625° regular grid, covering the period from 2019 to present (one day before real time). This product is built from optimal interpolating the Level-3C (merged single-sensor, L3C) SEVIRI data as observations and the CMEMS Mediterranean model analyses as first-guess.</p> 
Horizontal resolution	0.0625° x 0.0625° (1/16°) degrees [871x253]
Temporal resolution	Hourly
Spatial coverage	Mediterranean Sea + adjacent North Atlantic box (W=-18.1250, E=36.2500, S=30.2500, N=46.0000)
Temporal coverage	2019/01/01 – near real time (-14H)
Vertical level	<u>~1 mm (surface only)</u>
Variables	Sub-skin SST (K) Analysis Error (%)
Format	NetCDF – CF-1.4 convention compliant
DOI	https://doi.org/10.25423/CMCC/SST_MED_PHY_SUBSKIN_L4_NRT_010_036
Comments	Eventual updates of this product will be described in the corresponding Product User Manual (PUM) and Quality Information Document (QUID) available on the CMEMS on line catalogue.

Table 21. The CMEMS MED DOISST product description synthesis.

3.2 Background

The reconstruction of gap-free hourly mean SST fields is based on a blending of satellite observations and model analyses (used as first-guess/background) using optimal interpolation (OI), following the approach proposed by Marullo et al. (2014). The OI method determines the optimal solution to the interpolation of a spatially and temporally variable field with data voids, where “optimal” is intended in a least square sense (see e.g. Bretherton et al., 1976). The optimally interpolated variable, or analysis (F_a), is obtained as follows:

$$F_a(x, t) = F_b(x, t) + \sum_{i,j=1}^n W_{i,j} (F_{obs,i}(x, t) - F_b(x, t)) \quad (1)$$

In practice, the analysis $F_a(x, t)$ at a particular location in space and time (x, t) is obtained as a correction to a background field ($F_b(x, t)$). The correction is estimated as a linear combination of the observation anomalies ($F_{obs} - F_b$), where the coefficients $W_{i,j}$ are obtained by minimizing the analysis error variance.

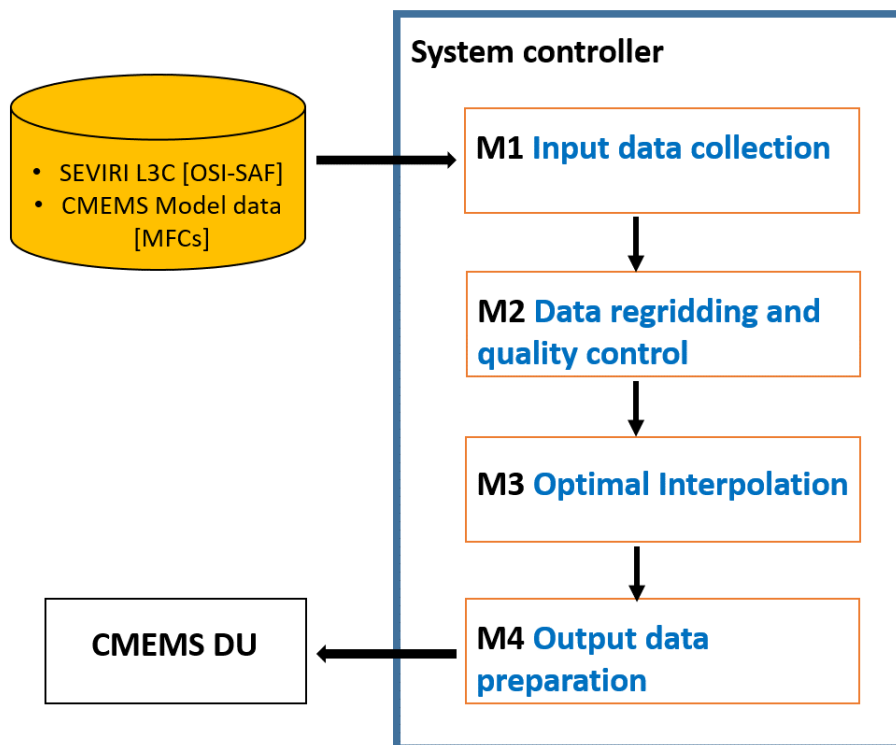
The choice of using a model output as first-guess represents the best alternative to the use of climatologies or previous analyses, as usually done by other schemes to produce daily SST L4 maps, since the model provides physically consistent estimates of hourly SSTs in the absence of any observation or in situ measurement (Marullo et al., 2014). In fact, the model takes into account the effect of air-sea interactions by imposing external forcings that drive momentum and heat exchanges at the upper boundary. As such, it is able to reproduce at least part of the diurnal warming effects, that are driven by the forcing diagnosed from atmospheric model analyses. Using the model output as a first-guess means we are treating the hourly satellite data as corrections to the hourly model data. These anomalies are generally small and mostly drive corrections to the spatial patterns, while displaying a reduced diurnal cycle. Anomaly data from different times of the day can thus be more “safely” used to build the interpolated field at each reference time (with different weights). Unfortunately, the first model layer is at 1 m depth, which means that it will generally underestimate the diurnal cycle anyway. While 1D models could in principle be used to better reproduce sub-skin SST from model data, the approach presented here is focusing on providing estimates that are as close as possible to the original satellite data, avoiding the complications of setting up an additional preprocessing step just to improve the first-guess.

3.3 Processing chain

The system implements the DOISST scheme developed by Marullo et al. (2014). The DOISST system ingests merged single-sensor (L3C) SEVIRI data as the observation source, and the CMEMS Mediterranean Sea model outputs (first layer) as first-guess. It has been shown that the diurnal signal in the hourly anomaly SST field (satellite-model) is reduced by about one order of magnitude with respect to the full signal, thus allowing to interpolate SST anomalies using satellite data acquired at different

277 ~~times of the day (Marullo et al., 2014). Several trials over a large variety of environmental conditions have shown that the~~
278 ~~temporal window to be used for the selection of input observations is ± 24 hours.~~

279 The data sub-sampling strategy, inversion technique and numerical implementation of the optimal interpolation scheme are
280 based on the CMEMS NRT MED SST processing chain (Buongiorno Nardelli et al., 2013), which provides daily mean fields
281 of foundation SST over the Mediterranean Sea (CMEMS product reference:
282 SST_MED_SST_L4_NRT_OBSERVATIONS_010_004, [https://resources.marine.copernicus.eu/product-](https://resources.marine.copernicus.eu/product-detail/SST_MED_SST_L4_NRT_OBSERVATIONS_010_004/INFORMATION)
283 [detail/SST_MED_SST_L4_NRT_OBSERVATIONS_010_004/INFORMATION](https://resources.marine.copernicus.eu/product-detail/SST_MED_SST_L4_NRT_OBSERVATIONS_010_004/INFORMATION); last access: 03 November 2021). Here, the
284 diurnal SST chain is organized in three main modules (Fig. 1).



285 **Figure 1.** Schematic diagram of the processing chain used for the MED DOISST SST product.
286

287

288 Module M1 manages the external interfaces to get both upstream L3C SST and model data: hourly mean L3C sub-skin SST
289 data at 0.05° grid resolution are downloaded from OSI-SAF; hourly seawater potential temperatures at 1.0182 meter are
290 obtained from the CMEMS Mediterranean Sea model outputs, [provided on a 0.042° regular grid](#).

291 Module M2 extracts and regrids (through bilinear interpolation) L3C data and model outputs over the CMEMS Mediterranean
292 Sea geographical area ([see Table 2](#)). A selection over SEVIRI is performed by flagging the pixels with quality flag < 3.

293 Module M3 performs a space-time optimal interpolation (OI) algorithm. L4 data are obtained as a linear combination of the
294 SST anomalies, weighted directly with their correlation to the interpolation point and inversely with their cross-correlation and
295 error ([Eq. 1](#)). Correlations are typically expressed through analytical functions with predefined spatial and temporal de-
296 correlation lengths. Here, the covariance function $f(r, \Delta t)$ is the one defined in Marullo et al. (2014), and given as the product
297 of a spatial and temporal component:

$$f(r, \Delta t) = \left[\alpha \cdot e^{-\frac{r}{R}} + \frac{1-\alpha}{(1+r)^c} \right] \cdot e^{-\left(\frac{\Delta t}{T}\right)^d} \quad (2)$$

300 where r is the distance (in km) between the observation and the interpolation point; Δt is the temporal difference (in hours)
301 between the observation and the interpolation point; R = 200 km is the decorrelation spatial length; T = 36 h is the decorrelation
302 time length; the other parameters are set as follows: a = 0.70, c = 0.26, d = 0.4. [All these parameters have been derived in](#)
303 [Marullo et al. \(2014\), deduced from a nonlinear least square fit between the estimated temporal and spatial correlations.](#)~~At~~
304 ~~these parameters have been deduced from a statistical analysis of the satellite SST data. In practice, the weights in expression~~
305 ~~(1) are computed directly from the analytical function (2).~~

306 The input data are selected only within a limited sub-domain (within a given space-time interval, [also called “influential”](#)
307 [radius](#)), with a temporal window of ± 24 h ([this the result of several trials over a large variety of environmental conditions;](#)
308 Marullo et al., 2014) and a spatial search radius of about 700 km (Buongiorno Nardelli et al., 2013). A check to avoid data
309 propagation across land is performed between each pixel within the sub-domain and the given interpolation point (eventually
310 discarded if there are land pixels between the straight line connecting the two points).

311 The interpolation error (analysis_error field in the L4 file, [Table 24](#)) is obtained from the formal definition of the error variance
312 derived from optimal interpolation theory (e.g., Bretherton et al., 1976). [This error ranges between 0-100%, meaning that the](#)
313 [error is almost zero when an optimal number of observations is present within the space-time influential radius, while only](#)
314 [first-guess data are used \(i.e. no observations are found within the search radius\) when the error is 100%. This error ranges](#)

~~between [0,100%], meaning that all observations are used (no first-guess data are used) when the error is zero, while only first-guess data are used (i.e. no observations available) when the error is 100%.~~

The optimal interpolation algorithm is synthesized as follows:

- Hourly SEVIRI and model SSTs in a space/time window of 700 km/ ± 24 h around the interpolation position/time are ingested;
- SEVIRI data with quality flag ≥ 3 are retained;
- Regridding over the Mediterranean Sea;
- Hourly model SSTs are subtracted from valid SSTs producing SST anomalies;
- SST anomalies are used as data input for the optimal interpolation analysis;
- Optimal interpolation is run using the covariance function defined above;
- The model SST is added to the optimally interpolated output again.

The only difference with the original method is that all the input observations are interpolated, while in Marullo et al. (2014) valid SST observations are left unchanged (not interpolated).

4 Validation of diurnal product

4.1 Validation framework

The accuracy of the MED DOISST product has been assessed through comparison with independent co-located (in space and time) surface drifting buoy data (matchups). The validation framework is based on the compilation of a matchup database between DOISST and drifters measurements covering the full years 2019 and 2020. The large number of drifters provides a rather homogeneous and continuous spatial and temporal coverage over the whole period (Fig. 2) allowing a robust statistical approach.

Firstly, a pre-selection of high-quality drifter data is performed, retaining only temperatures with quality flag equal to 1 (good) or 2 (probably good) (see section 2.3). Then, the ~~validation-co-location~~ is carried out on hourly basis, building a matchup database by collecting the closest (in space) SST grid point to the in situ measurement within a symmetric temporal window of 30 minutes with respect to the beginning of each hour. A final quality ~~outlier detection check~~~~control~~ ~~iteratively is carried out by~~ identifying drifter ~~temperatures-data~~ for which the module of the difference ~~with respect to satellite observations between satellite and drifter temperature~~ exceeds n -times the standard deviation σ of the distribution of ~~all these the~~ differences (δ). At each step ~~n decreases of decreasing n, and~~ data that falls out of the interval $I = [mean(\delta) - n \cdot \sigma, mean(\delta) + n \cdot \sigma]$ are flagged as outliers and ~~then not included in the next step~~ removed. ~~For each n, the selected outliers are eliminated and the process is repeated for the same value of n until no more outliers are detected. Then the system moves~~

345 ~~to n-1.~~ The process starts for n=10 and stops at n=3, ~~and.~~ ~~This last quality control~~ removes ~1% of the total original sampling
346 (as expected from a gaussian distribution) of drifter data that clearly revealed anomalous temperature values.

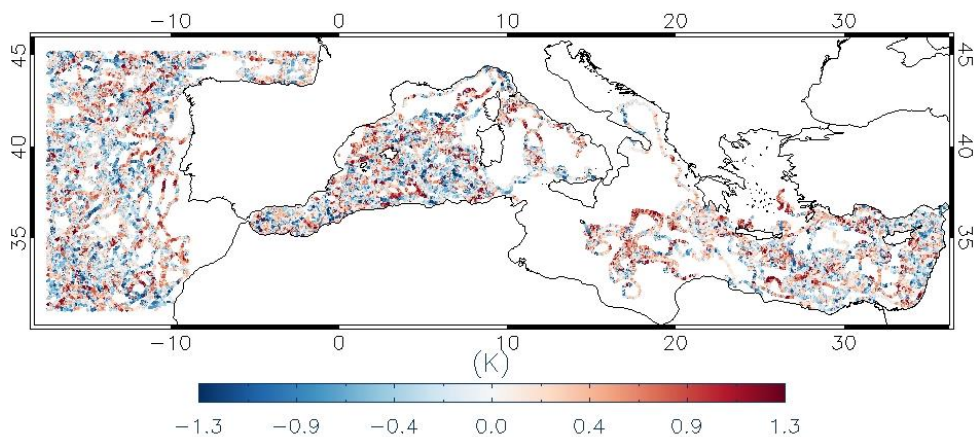
347 ~~The main v~~Validation statistics are quantified in terms of mean bias and Root-Mean-Square Difference (RMSD) from matchup
348 temperature differences (namely, SST minus drifter). Each statistical parameter is associated with a 95% confidence interval
349 computed through a bootstrap procedure (Efron 1994).

350 In order to evaluate the DOISST performance with respect to the model, the same validation procedure has been applied to the
351 ~~modeled~~modelled SST.
352

353 4.2 Comparison with drifters

354 4.2.1 The mean diurnal cycle

355 The spatial distribution of DOISST and drifter matchups over the 2019-2020 period, along with their pointwise ~~bias-difference~~
356 (i.e., DOISST minus drifter measurement) shows a rather homogeneous coverage over the most of the CMEMS MED domain
357 (Fig. 2), although some areas are characterized by quite low coverage, such as the North Adriatic Sea or North Aegean Sea.
358 The spatial distribution also evidences ~~the predominance of a positive tendency of the bias,~~ indicating that, ~~on average,~~
359 DOISSTs are warmer than drifters' temperatures ~~on average.~~



360
361 **Figure 2.** Spatial distribution of the matchup points along with their punctual bias (i.e., SST minus drifter data, K) over the
362 CMEMS Mediterranean domain from 2019/01/01 to 2020/12/31.
363

364
365
366
367
368

The DOISST product shows effectively an overall small positive mean bias of 0.041 ± 0.001 K and a RMSD of 0.412 ± 0.001 K (Table 2). A negative bias of -0.100 ± 0.001 K and slightly larger RMSD of 0.467 ± 0.001 K characterize model SSTs. [Both DOISST and the model show high and comparable correlation coefficients \(more than 0.99\).](#)

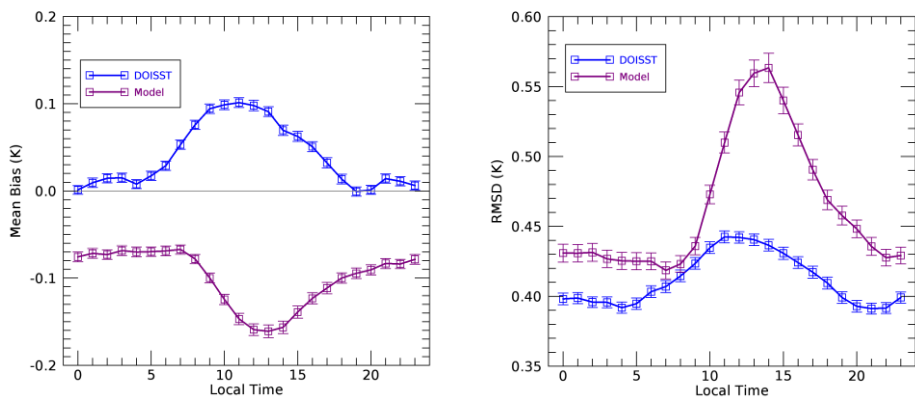
	Period	Mean bias (K)	RMSD (K)	Correlation coeff.	Matchups
DOISST	2019-01-01 to 2020-12-31	0.041 ± 0.001	0.412 ± 0.001	0.992	548959
Model	2019-01-01 to 2020-12-31	-0.100 ± 0.001	0.467 ± 0.001	0.991	548959

369
370
371

Table 32. Summary statistics of DOISST and model outputs. Mean bias (K), [and](#) RMSD (K), [and](#) correlation coefficient are derived from temperature differences against drifters' data over the period 2019-2020. [Each statistical parameter is associated with a 95% confidence interval computed through a bootstrap procedure \(Efron 1994\).](#)

372
373
374
375
376
377
378
379
380

The hourly mean bias of DOISST and model shows similar but opposite behaviour (Fig. 3, and Table 43). In both cases, the bias clearly exhibits a diurnal oscillation during the 24 hours but, while the bias of DOISST increases positively during the central diurnal warming hours, the one of the model increases negatively. The DOISST mean bias is practically null between 17:00 to 06:00 local time, ranging between -0.001 and 0.03 K, and highest (~ 0.1 K) between 10:00 and 13:00 local time. The bias of the model oscillates around ~ -0.07 K between 23:00 and 07:00 local time. Then, it increases (in absolute value) reaching the peak of ~ -0.16 K between 11:00 and 14:00 and decreases successively. Similar results are obtained for the RMSD, which increases with diurnal warming (Fig. 3, Table 43). However, the RMSD of DOISST is less impacted by diurnal variations, characterized by an amplitude of ~ 0.04 K against ~ 0.14 K of the model.



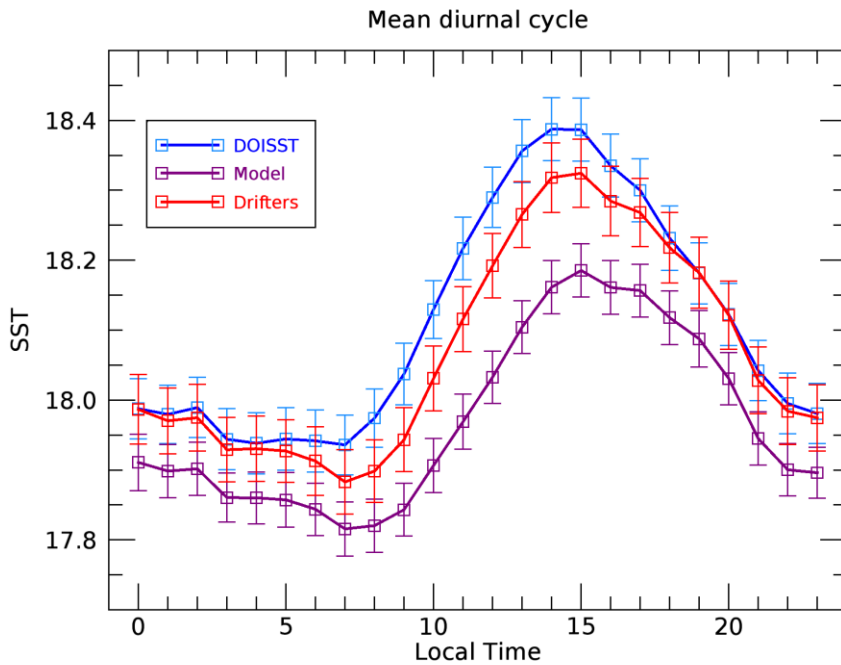
381 **Figure 3.** Mean bias (K) and RMSD (K) relative to MED DOISST (blue line) and model (purple line) based on the differences
 382 against drifters' data. Mean bias and RMSD are given as hourly mean over the period 2019-2020.

Hour (local time)	Mean BIAS (K) (DOISST)	RMSD (K) (DOISST)	BUOY-AVAIL	Mean BIAS (K) (Model)	RMSD (K) (Model)
HH: 00	0.001 ± 0.005	0.398 ± 0.004	22807	-0.076 ± 0.006	0.431 ± 0.006
HH: 01	0.009 ± 0.005	0.399 ± 0.004	23004	-0.072 ± 0.006	0.431 ± 0.006
HH: 02	0.014 ± 0.005	0.396 ± 0.004	22798	-0.073 ± 0.005	0.431 ± 0.006
HH: 03	0.015 ± 0.005	0.396 ± 0.004	23078	-0.068 ± 0.006	0.427 ± 0.006
HH: 04	0.008 ± 0.005	0.392 ± 0.004	22857	-0.070 ± 0.005	0.425 ± 0.006
HH: 05	0.017 ± 0.005	0.395 ± 0.004	22806	-0.070 ± 0.005	0.425 ± 0.006
HH: 06	0.029 ± 0.005	0.403 ± 0.004	22819	-0.069 ± 0.006	0.425 ± 0.006
HH: 07	0.053 ± 0.005	0.407 ± 0.004	23379	-0.067 ± 0.005	0.419 ± 0.006
HH: 08	0.076 ± 0.005	0.415 ± 0.004	23501	-0.078 ± 0.006	0.423 ± 0.006
HH: 09	0.094 ± 0.005	0.423 ± 0.004	23481	-0.100 ± 0.006	0.436 ± 0.006
HH: 10	0.099 ± 0.006	0.435 ± 0.004	23270	-0.125 ± 0.006	0.473 ± 0.007
HH: 11	0.101 ± 0.006	0.442 ± 0.004	23311	-0.147 ± 0.006	0.510 ± 0.007
HH: 12	0.098 ± 0.006	0.442 ± 0.004	23129	-0.159 ± 0.007	0.546 ± 0.009
HH: 13	0.091 ± 0.006	0.440 ± 0.005	22836	-0.161 ± 0.007	0.560 ± 0.009
HH: 14	0.070 ± 0.006	0.436 ± 0.004	22673	-0.157 ± 0.007	0.563 ± 0.011
HH: 15	0.062 ± 0.006	0.431 ± 0.004	22418	-0.139 ± 0.007	0.540 ± 0.009
HH: 16	0.051 ± 0.006	0.424 ± 0.004	22368	-0.123 ± 0.007	0.515 ± 0.008
HH: 17	0.032 ± 0.006	0.417 ± 0.004	22019	-0.111 ± 0.006	0.491 ± 0.007
HH: 18	0.014 ± 0.006	0.410 ± 0.004	21916	-0.100 ± 0.006	0.469 ± 0.007
HH: 19	-0.001 ± 0.005	0.399 ± 0.004	22117	-0.095 ± 0.006	0.458 ± 0.007
HH: 20	0.001 ± 0.005	0.393 ± 0.004	22458	-0.090 ± 0.006	0.448 ± 0.006
HH: 21	0.014 ± 0.005	0.391 ± 0.004	23229	-0.083 ± 0.005	0.436 ± 0.006
HH: 22	0.011 ± 0.005	0.392 ± 0.004	23272	-0.084 ± 0.006	0.428 ± 0.006
HH: 23	0.006 ± 0.005	0.399 ± 0.004	23413	-0.078 ± 0.006	0.429 ± 0.006

Table 43. Summary statistics of MED DOISST and model products based on the differences against drifters' data over the matchup points. Mean bias (K), RMSD (K) and number of matchups are given as hourly mean over the period 2019-2020. Each statistical parameter is associated with a 95% confidence interval computed through a bootstrap procedure (Efron 1994).

The mean diurnal cycle of DOISST (namely, the 24-hour mean SSTs estimated over the matchup dataset) is in very good agreement, within the error confidence interval, with the SST cycle reconstructed from drifters (Fig. 4). The two diurnal cycles are practically coincident-unbiased between 17:00 and 06:00, while they are biased by ~ 0.1 K between sunrise and 16:00, coherently with the DOISST bias oscillation (Fig. 3). This bias could be related to skin SST getting warmer faster than the temperature at 20 cm depth ~~20 cm temperature~~. The diurnal cycle of model SST maintains always below that of in situ

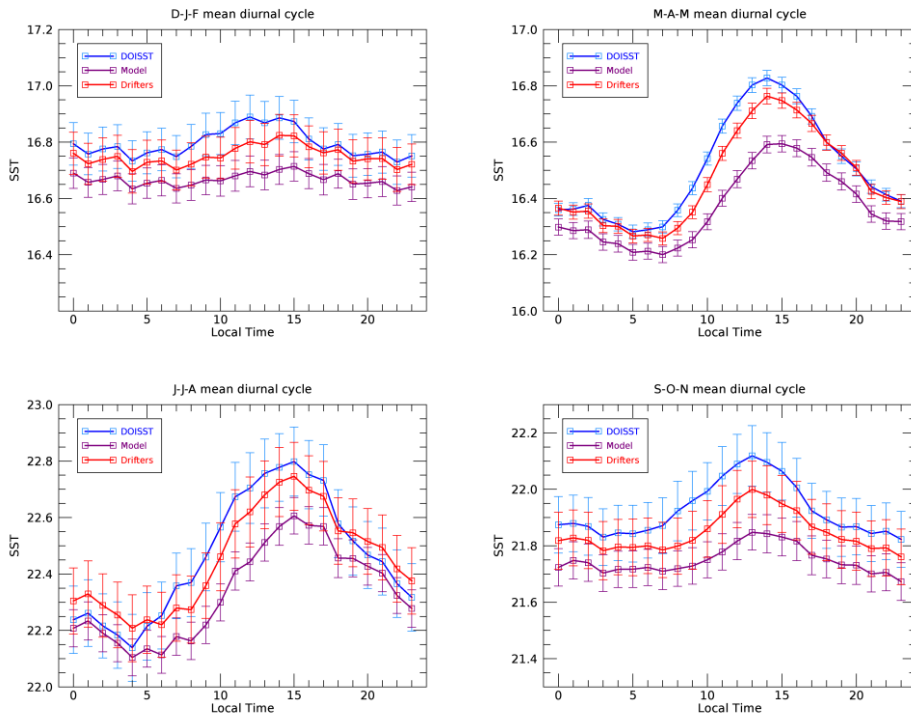
393 temperatures, evidencing larger differences during the central diurnal warming hours (Fig. 4). However, apart from the biases
394 likely induced by the different depths, the SST amplitude as estimated from the DOISST and the model is $\sim 2.3\%$ larger and
395 $\sim 16\%$ smaller than that of drifters, respectively, suggesting that the model tends to underestimate diurnal variations.



396 **Figure 4.** Mean diurnal cycle for MED DOISST (blue line), model (purple line) and drifters (red line) computed over the
397 matchups from 2019 to 2020.
398
399

400 A delay of ~ 1 hour of the model with respect to DOISST and in situ on the onset of diurnal warming and in reaching the
401 maximum is also evident. This delay could be explained as the physical result of delayed solar heating of the skin layer sensed
402 by the satellite and of the first model layer. This may also be a consequence of the different packaging of the SEVIRI and
403 model SST data into the hourly files: model hourly SST fields are centered at half of every hour (e.g., 12:30), while SEVIRI
404 L3C at the beginning of each hour (e.g., 12:00) and obtained from collating data within one hour (from 11:30 to 12:29).

405 The capability of DOISST to capture and realistically reproduce diurnal variability is further investigated by analysing the
 406 seasonally averaged SST diurnal cycle (Fig. 5), computed as for the mean diurnal cycle (by using the matchup dataset) but
 407 over seasons: winter (December to February, D-J-F), spring (March to May, M-A-M), summer (June to August, J-J-A) and
 408 autumn (September to November, S-O-N). The effect of warming in the diurnal SST excursion is clearly more pronounced
 409 during spring and summer than winter and autumn, and reconstructed well in DOISST. During the warmer seasons, the
 410 DOISST shows the lower biases (Table 54), estimated in 0.036 ± 0.001 K (spring) and 0.012 ± 0.003 K (summer). Conversely,
 411 the model reaches its higher biases, namely -0.101 ± 0.001 K (spring) and -0.117 ± 0.003 K (summer). The good agreement
 412 between DOISST and drifters during winter and autumn (Table 54) reveals that the hourly DOISST fields are reconstructed
 413 accurately also under cloudy conditions, which are more frequent during these seasons (Kotsias and Lolis, 2018).



414
 415 **Figure 5.** Seasonal mean diurnal cycle over the period 2019-2020 for MED DOISST (blue line), model (purple line) in situ
 416 (red line).

	Period	Mean bias (K)	RMSD (K)	Matchups
D-J-F	DOISST	0.045 ± 0.003	0.428 ± 0.002	90247
	Model	-0.084 ± 0.004	0.563 ± 0.003	
M-A-M	DOISST	0.036 ± 0.001	0.383 ± 0.001	308448
	Model	-0.101 ± 0.001	0.389 ± 0.002	
J-J-A	DOISST	0.012 ± 0.003	0.483 ± 0.002	74107
	Model	-0.117 ± 0.003	0.486 ± 0.004	
S-O-N	DOISST	0.079 ± 0.003	0.429 ± 0.002	76157
	Model	-0.098 ± 0.004	0.590 ± 0.004	

Table 54. Summary statistics of DOISST and model outputs. Mean bias (K) and RMSD (K) are derived from temperature differences against drifters' data during winter (D-J-F), spring (M-A-M), summer (J-J-A) and autumn (S-O-N) over the period 2019-2020. Each statistical parameter is associated with a 95% confidence interval computed through a bootstrap procedure (Efron 1994).

The capability of DOISST to reproduce diurnal warming events is analysed in the following section.

4.2.2 Diurnal warming events

Diurnal warming (DW) can be defined as the ~~(positive)~~ difference between the SST at a given time of the day and the foundation SST (see e.g. Minnett et al., 2019), i.e. the water temperature at a depth such that the daily variability induced by the solar irradiance is negligible. In many cases, the foundation SST coincides with the night minimum SST, namely the temperature that is recorded just before sunrise.

The capability of DOISST to describe diurnal warming events is analysed here in comparison with SEVIRI L3C, OSTIA diurnal, model and drifter data. The evaluation is carried out by computing daily Diurnal Warming Amplitudes (DWAs) from drifters and building a matchup dataset of DWAs as estimated from DOISST, SEVIRI L3C, OSTIA and model data. The inclusion of SEVIRI data is mainly aimed at evaluating the impact of optimal interpolation on the input SEVIRI SSTs, while OSTIA diurnal is used as intercomparison product. The ~~diurnal warming amplitude (DWA)~~ is estimated here as a difference between the maximum occurred during daytime (10:00-18:00 local time) and the minimum during nighttime (00:00-06:00 local time) (see also Takaya et al., 2010; While et al., 2017). Explicitly, for each day (from 2019 to 2021) and for each drifter the two positions and times relative to the minimum and maximum temperature are stored; over the same times and nearest

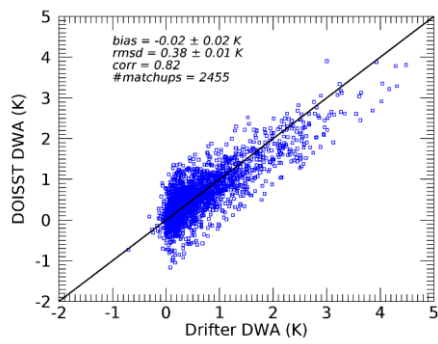
439 positions, the temperatures of the other datasets are stored too. The grid resolution of OSTIA diurnal (namely, 0.25° deg.) has
440 been left unchanged since what is needed is just the SST value at a given position, the nearest to the drifter's one.

441 The scatter plots of DOISST, SEVIRI, OSTIA, and model vs in situ-measured DWA have been computed for the years 2019-
442 2020 (Fig. 6) and organized during spring-summer and winter-autumn seasons (Fig. 7). This choice is aimed at comparing the
443 behaviour of the ~~three-four~~ products as a function of the seasons, since larger DWA intensities are expected in the spring-
444 summer period.

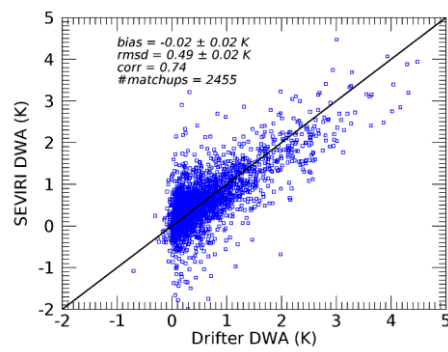
445 Overall, there is a good agreement between DOISST and drifter DWAs (Fig. 6a) as confirmed by an almost null mean bias (-
446 0.02 K), low RMSD (0.38 K) and high correlation coefficient (0.82). The largest DW amplitudes reach values as high as 4 K
447 in both DOISST and drifter data. SEVIRI (Fig. 6b) shows the same bias (-0.02 K) of DOISST in reconstructing DWAs but
448 higher RMSD (0.49 K) and lower correlation (0.74). It is relevant to note that the spread of SEVIRI DWAs around the line of
449 perfect agreement is reduced in DOISST, which coherently has a lower RMSD. The model (Fig. 6c) clearly underestimates
450 diurnal amplitudes larger than 1 K, and it is characterized by the highest a high mean bias (-0.23 K) and RMSD (0.5566 K),
451 and lowest correlation coefficient (0.66). Similarly, OSTIA diurnal (Fig. 6d) underestimates DWAs larger than 1 K, and it is
452 characterized by the highest mean bias (-0.28 K), RMSD of 0.54 K but shows less dispersion than the model around the line
453 of perfect agreement (correlation of 0.72).

454 The majority of DWA events lie between 0-1 K all over the year, but higher values are effectively reached during spring and
455 summer (Fig. 7). During these seasons, it appears more evident the capability of DOISST to better describe DWAs larger than
456 1 K (mean bias = -0.04 K; RMSD = 0.42 K; corr. = 0.83) compared to SEVIRI (mean bias = -0.05 K; RMSD = 0.53 K; corr.
457 = 0.76) and especially to the model (mean bias = -0.27 K; RMSD = 0.65 K; corr. = 0.63) and OSTIA diurnal (mean bias = -
458 0.39 K; RMSD = 0.66 K; corr. = 0.71). During winter and autumn, the overall statistics of the four products get better, clearly
459 due to the fact that the majority of DWA events range between 0-0.5 K. However, A similar behaviour is obtained during
460 winter and autumn when-DWA events exceeding 1 K are also observed, and such intense amplitudes are not found in the
461 model-derived and OSTIA DWAs. Additionally, the good agreement between DOISST and drifters still confirms that
462 interpolated data do not suffer from the increased cloud cover during winter and autumn periods.

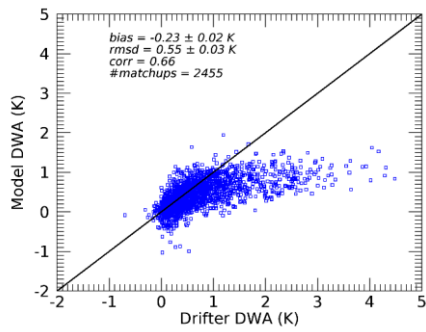
(a)



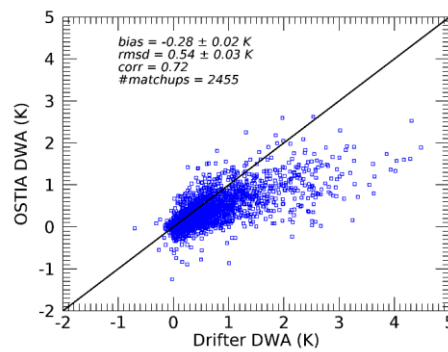
(b)



(c)



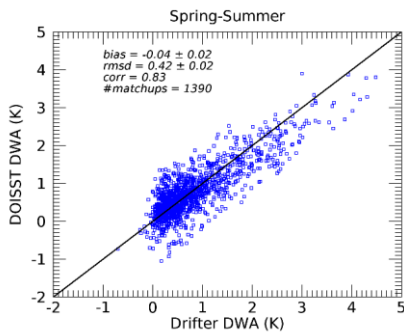
(d)



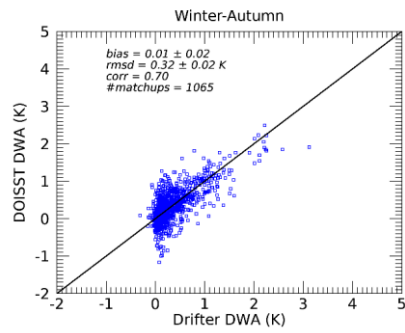
468 **Figure 6.** DWA scatter plots for (a) DOISST, (b) SEVIRI L3C_ and (c) model_ and (d) OSTIA diurnal vs drifters over the
469 period 2019-2020.

470
471
472
473
474
475

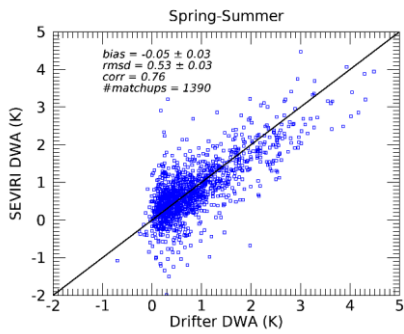
(a)



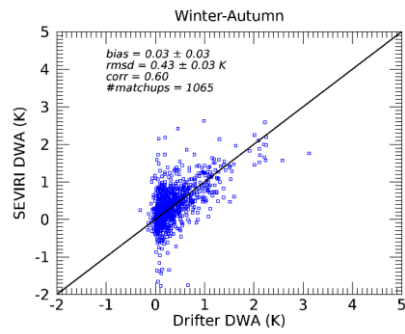
(b)



(c)

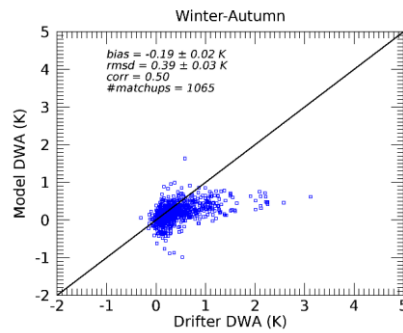
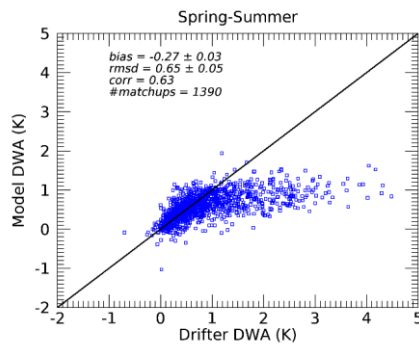


(d)



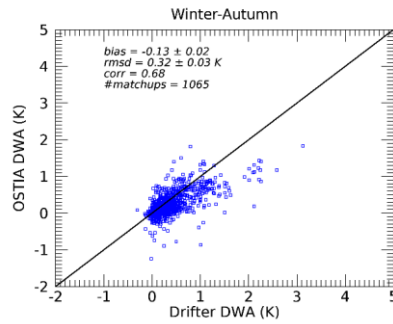
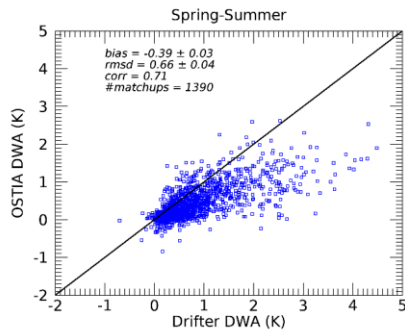
(e)

(f)



(g)

(h)



477
478
479
480

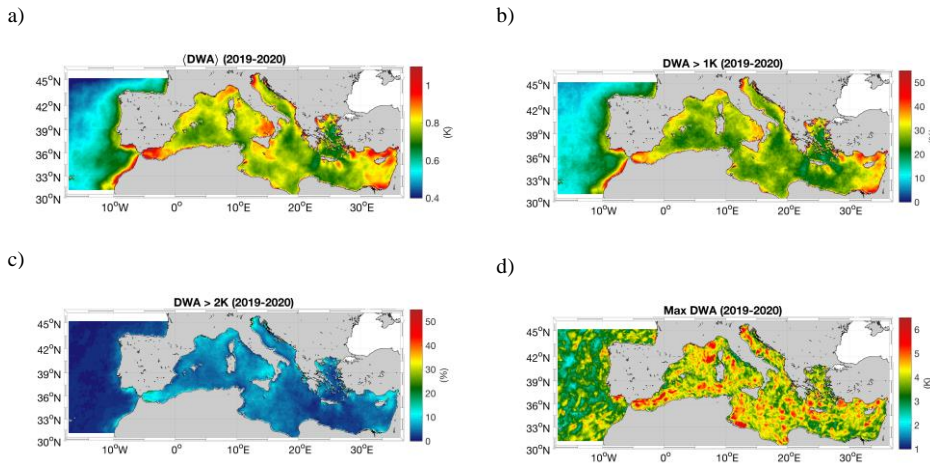
Figure 7. DWA scatter plots for DOISST (a,b), SEVIRI L3C (c,d), and model (e,f), and OSTIA diurnal (g,h) vs drifters during Spring (M-A-M) and Summer (J-J-A), and Winter (D-J-F) - Autumn (S-O-N), over the period 2019-2020.

481 Having demonstrated the reliability of DOISST in the DWA estimate, we analyze its capability to reproduce the typical spatial
482 variability and intensity of DW events in the Mediterranean Sea, a basin characterized by a frequent occurrence of intense DW
483 events (Böhm et al., 1991; Buongiorno Nardelli et al., 2005; Gentemann et al., 2008; Merchant et al., 2008). In our investigation
484 area, the 2019-2020 mean DWA ranges from a minimum of 0.4 K in the Atlantic ocean box off the Strait of Gibraltar, to a
485 maximum of 1.2 K in several regions of the Mediterranean Sea (Fig. 8a) where individual diurnal warming events exceeding
486 1 or even more than 2 K are quite frequent. The largest DWA were observed in the Levantine Basin, in the North Adriatic Sea
487 and in correspondence with the Alboran Gyre. Less intense, though still remarkable, mean DWA patches reaching 0.9 K are
488 found around the southern tip of the Italian Peninsula as well as in the coastal Ligurian Sea. In the same areas, it is found that

489 the frequency of DW events larger than 1 K and 2 K can reach up to 55% and 10% of the analyzed time series, respectively
 490 (bearing in mind that our time series is given by the total number of days in 2019 and 2020) (Fig. 8b-c). [The spatial variability](#)
 491 [and magnitude of the DWA described by the DOISST product are consistent with past and recent studies on the SST diurnal](#)
 492 [variability in the Mediterranean Area \(Minnet et al. 2019; Marullo et al. 2016; Marullo et al. 2014\).](#)

493

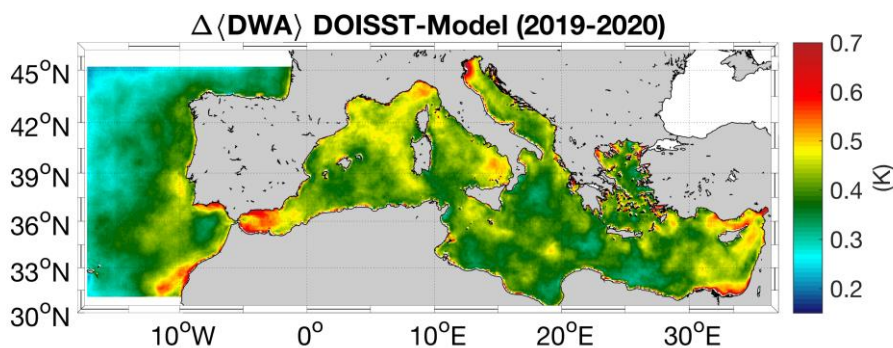
494 The magnitude of the maximum SST diurnal oscillation is also investigated. The spatial distribution of the maximum DWA
 495 observed through 2019-2020 in the Mediterranean Sea (6°W to 36°E and 30°N to 46°N) (Fig. 8d) shows that the largest
 496 amplitudes reach and exceed 3 K in 98% of the basin and local DWA patches exceeding 6 K are also ubiquitous, confirming
 497 that the Mediterranean is one of the areas with the largest DWs of the global ocean (Minnet et al. 2019, and references therein).



498 **Figure 8.** a) Mean diurnal warming amplitude (DWA) derived from DOISST; b) Percentage (over the total number of days in
 499 the 2019-2020 period) of DOISST DWA larger than 1 K; c) Percentage of DOISST DWA larger than 2 K; d) Maximum
 500 observed DOISST DWA. All the maps refer to the 2019-2020 period.
 501
 502

503 When compared to the model, DOISST exhibits mean DWAs with larger intensity than model outputs in all the locations of
 504 the study area (Fig. 9). The Δ DWA, defined as $DWA_{DOISST} - DWA_{Model}$, is always larger than 0.2 K and locally reaches
 505 extreme values of ~ 1 K. The extent of the Δ DWA generally increases in areas where the DOISST mean DWA is larger, such

506 as in the Alboran Sea, Ligurian Sea, Levantine Basin and Southern Tyrrhenian, suggesting a tendency of the model to
507 underestimate the largest DW events.



508 **Figure 9.** Mean amplitude of the SST DW. Differences between the mean DWA seen by the DOISST product and the
509 model outputs (first layer).
510
511

512 5 Data availability

513 The Mediterranean diurnal optimal interpolated SST product is distributed as part of the CMEMS catalogue, and identified as
514 SST_MED_PHY_SUBSKIN_L4_NRT_010_036 (CMEMS product reference) and cmems_obs-sst_med_phy-
515 sst_nrt_diurnal-oi-0.0625deg_PT1H-m (CMEMS dataset reference) ([https://resources.marine.copernicus.eu/product-
516 detail/SST_MED_PHY_SUBSKIN_L4_NRT_010_036/INFORMATION](https://resources.marine.copernicus.eu/product-detail/SST_MED_PHY_SUBSKIN_L4_NRT_010_036/INFORMATION), last access: 03 November 2021,
517 https://doi.org/10.25423/CMCC/SST_MED_PHY_SUBSKIN_L4_NRT_010_036; Pisano et al, 2021). Access to the product
518 is granted after free registration as a user of CMEMS at <https://resources.marine.copernicus.eu/registration-form> (last access:
519 03 November 2021). Once registered, users can download the product through a number of different tools and services,
520 including the web portal Subsetter, Direct-GetFile (DGF) and FTP. A Product User Manual (PUM) and QUality Information
521 Document (QUID) are also available as part of the CMEMS documentation ([https://resources.marine.copernicus.eu/product-
522 detail/SST_MED_PHY_SUBSKIN_L4_NRT_010_036/DOCUMENTATION](https://resources.marine.copernicus.eu/product-detail/SST_MED_PHY_SUBSKIN_L4_NRT_010_036/DOCUMENTATION), last access: 03 November 2021). Eventual
523 updates of the product will be reflected in these documents. The basic characteristics of the DOISST product are summarized

524 in Table 24. The reduced subset used here for validation and review purposes is openly available at
525 <https://doi.org/10.5281/zenodo.5807729> (Pisano, 2021).

527 6 Summary and conclusions

528 A new operational Mediterranean diurnally varying SST product has been released (May 2021) within the Copernicus Marine
529 Environment Monitoring Service (CMEMS). This dataset provides optimally interpolated (L4) hourly mean maps of sub-skin
530 SST over the Mediterranean Sea at 1/16° horizontal resolution, covering the period from 1st January 2019 to near real time (1
531 day before real time) (Pisano et al., 2021). The diurnal optimal interpolated SST (DOISST) product is obtained from a blending
532 of hourly satellite (SEVIRI) data and model outputs via optimal interpolation, where the former are used as the observation
533 source and the latter as background. This method has been firstly proposed by Marullo et al. (2014), validated over one year
534 (2013) in Marullo et al. (2016), and implemented here operationally. The validation of the operational product was also
535 extended over two years (2019-2020).

536 In an ideal case, all data would be generated and compared at the same depth. Unfortunately, the first model layer is centered
537 at 1 m depth, while sub-skin SST is, by definition, representative of a depth of ~1 mm. In principle, it could be possible to
538 correct all the data, bringing them all to the same depth before any comparison or merging, by applying some model (see e.g.
539 Zeng et al., 1999). However, any correction algorithm would have added potential uncontrolled error sources (e.g., related to
540 ancillary data and/or to model assumptions) and implied significant additional operational efforts. For these reasons, rather
541 than trying to correct the first-guess bias, we preferred to leave it uncorrected, and focus on optimising the corrections driven
542 by available hourly satellite data.

543 DOISST proved to be rather accurate when compared to drifter measurements, and correctly reproduced the diurnal variability
544 in the Mediterranean Sea. The accuracy of DOISST results in an overall, almost null, mean bias of ~0.04 K and RMSD of
545 ~0.41 K (Table 32). This product is also more accurate than the input model, which shows a mean bias of ~-0.1 K and RMSD
546 of ~0.47 K. A warm (positive) and cold (negative) bias characterizes the DOISST and the model, respectively, also during
547 seasons (Fig. 5). These opposite biases are likely related to the different nature of the SST provided by DOISST, model and
548 drifter data, i.e. sub-skin (~1 mm upper first millimeters from the surface), averaged 1 m depth and 20 cm depth, respectively,
549 and then consistent with the physical consequence of a reduction of the temperature with depth due to the vertical transfer heat
550 process. The DOISST RMSD generally keeps lower values compared to the model, ranging from a minimum of ~0.40 K (vs
551 ~0.42 K for the model) to a maximum of ~0.44 K (vs ~0.56 K for the model).

552 Compared to its native version (Marullo et al., 2016), the DOISST product maintains the same RMSD (estimated in 0.42 K)
553 but displays a lower mean bias (estimated as -0.10 K). The reduced bias could be ascribed to the fact that valid SEVIRI SST

554 values are always interpolated in DOISST, while they are left unchanged in the original method. Additionally, the DOISST
555 bias is comparable with that estimated for SEVIRI over the Mediterranean Sea (-0.03 K; Marullo et al. 2016), while the
556 DOISST RMSD is rather lower than SEVIRI one (0.47 K; Marullo et al. 2016). The DOISST bias is also lower than that of
557 the OSTIA diurnal product, which produces gap-free hourly mean fields of skin SST for the global ocean, and has been found
558 to underestimate the diurnal range of skin SST by 0.1-0.3 °C (While et al., 2017).

559 The analysis of the SST diurnal cycle as estimated from both DOISST, model and drifter data shows that the diurnal oscillation
560 in SST is well reconstructed by the DOISST while the model tends to underestimate this amplitude mainly during the central
561 warming hours (Fig. 4), and during spring and summer (Fig. 5). Specifically, DOISST overestimates the mean diurnal
562 amplitude by ~2.3% compared to that of drifters, while the model underestimates it by ~16%. This is particularly evident in
563 the analysis of diurnal warming (DW) events, where diurnal warming amplitudes (DWAs) as estimated by DOISST, model,
564 and SEVIRI, and OSTIA diurnal data are compared vs drifter-derived DWAs. This analysis shows that amplitudes exceeding
565 1 K, as measured by drifters, are well reconstructed by DOISST (Fig. 6a) with a mean bias of ~-0.02 K and RMSD of ~0.38
566 K. The comparison with reconstructed SEVIRI DWAs (Fig. 6b) demonstrates that optimal interpolation does not change the
567 SEVIRI bias, which is practically null for both SEVIRI and DOISST (~-0.02 K), while it reduces the SEVIRI RMSD, from
568 ~-0.49 K (SEVIRI) to ~0.38 K (DOISST). This is also evident in the reduction of the spread of SEVIRI DWAs around the line
569 of perfect agreement (Fig. 6b). Both the model and OSTIA diurnal underestimate DWAs when exceeding 1 K with a mean
570 bias of ~-0.23 K (model, Fig. 6c) and ~-0.28 K (OSTIA, Fig. 6d), and RMSD of ~0.55 K for both products, while model SSTs
571 show significantly lower values, with a mean bias of ~-0.23 K (Fig. 6e). This underestimation could be related to several
572 factors, such as that the vertical resolution of the model does not resolve the vertical temperature profile within the warm layer.
573 Yet, the physics and atmospheric forcing and/or the assimilation implemented in the model and OSTIA, though different, are
574 only partially able to resolve diurnal variations larger than 1 K. In any case, we can argue that the tendency of the model to
575 underestimate DWAs, mainly for amplitudes > 1 K, does not strongly impact the performance of DOISST in reconstructing
576 these amplitudes. This is likely due to two concurrent factors, the high accuracy of SEVIRI SST data and that the Mediterranean
577 area is particularly advantageous in terms of clear sky conditions. The underestimation of the diurnal warming amplitude
578 (DWA) by the model could be related to several factors, such as that the vertical resolution does not resolve the vertical
579 temperature profile within the warm layer, the physics and atmospheric forcing implemented in the model, and/or the
580 assimilation of the foundation SST fields used for the correction of surface heat flux.

581 The comparison with reconstructed SEVIRI DWAs (Fig. 6b) demonstrates that optimal interpolation does not change the
582 SEVIRI bias, which is practically null for both SEVIRI and DOISST (~-0.02 K), while it reduces the SEVIRI RMSD, from
583 ~-0.49 K (SEVIRI) to ~0.38 K (DOISST). Finally, the seasonal analysis also reveals that DOISST is not impacted by the
584 different environmental conditions in the Mediterranean Sea, in particular from the much frequent cloudiness during winter
585 and autumn periods.

586 Overall, the DOISST product is able to accurately reconstruct the SST diurnal cycle, including diurnal warming events, for the
587 Mediterranean Sea and can thus represent a valuable dataset to improve the study of those processes that require sub-daily
588 frequency.

589
590

591 **Financial Support**

592 This work has been carried out within the Copernicus Marine Environment Monitoring Service (CMEMS) Sea Surface
593 Temperature Thematic Assembly Centre (SST TAC), contract n° 78-CMEMS-TAC-SST. This contract is funded by Mercator
594 Océan International as part of its delegation agreement with the European Union, represented by the European Commission,
595 to set-up and manage CMEMS.

596

597 **References**

598 Artale, V., Iudicone, D., Santoleri, R., Rupolo, V., Marullo, S., D'Ortenzo, F.; Role of surface fluxes in ocean general
599 circulation models using satellite sea surface temperature: validation of and sensitivity to the forcing frequency of the
600 Mediterranean thermohaline circulation; *J. Geophys. Res-Oceans*, 107(C8), 29-1–29-24,
601 <https://doi.org/10.1029/2000JC000452>, 2002

602 Bernie, D. J., Guilyardi, E., Madec, G., Slings, J. M., Woolnough, S. J., and Cole, J. Impact of resolving the diurnal cycle in
603 an ocean–atmosphere GCM. Part 2: A diurnally coupled CGCM. *Clim. Dynam.*, 31(7), 909-925, DOI 10.1007/s00382-008-
604 0429-z, 2008

605 Böhm, E., Marullo, S., and Santoleri, R.. AVHRR visible-IR detection of diurnal warming events in the western Mediterranean
606 Sea, *Int. J. Remote Sens.*, 12(4), 695-701, <https://doi.org/10.1080/01431169108929686>, 1991

607 Bowen, M. M., Emery, W. J., Wilkin, J. L., Tildesley, P. C., Barton, I. J., and Knewtson, R.. Extracting multiyear surface
608 currents from sequential thermal imagery using the maximum cross-correlation technique, *J. Atmos. Ocean. Tech.*, 19(10),
609 1665-1676, [https://doi.org/10.1175/1520-0426\(2002\)019%3C1665:EMSCFS%3E2.0.CO;2](https://doi.org/10.1175/1520-0426(2002)019%3C1665:EMSCFS%3E2.0.CO;2), 2002.

610 Bretherton, F. P., Davis, R. E., and Fandry, C. B.. A technique for objective analysis and design of oceanographic experiments
611 applied to MODE-73. In *Deep Sea Research and Oceanographic Abstracts*, 23, 7, 559-582, [https://doi.org/10.1016/0011-
612 7471\(76\)90001-2](https://doi.org/10.1016/0011-7471(76)90001-2), 1976..

613 Buongiorno Nardelli, B.; Marullo, S.; Santoleri, R.. Diurnal Variations in AVHRR SST Fields: A Strategy for Removing
614 Warm Layer Effects from Daily Images. *Remote Sens. Environ.*, 95 (1), 47–56. <https://doi.org/10.1016/j.rse.2004.12.005>,
615 2005

616 Buongiorno Nardelli, B., Tronconi, C., Pisano, A., and Santoleri, R.. High and Ultra-High resolution processing of satellite
617 Sea Surface Temperature data over Southern European Seas in the framework of MyOcean project. *Remote Sens. Environ.*,
618 129, 1-16. <https://doi.org/10.1016/j.rse.2012.10.012>, 2013

619 Chen, S. S., and Houze Jr, R. A. Diurnal variation and life-cycle of deep convective systems over the tropical Pacific warm
620 pool. *Q. J. Roy. Meteor. Soc.*, 123(538), 357-388, <https://doi.org/10.1002/qj.49712353806>, 1997

621 Clayson, C. A., and Bogdanoff, A. S.. The effect of diurnal sea surface temperature warming on climatological air–sea fluxes.
622 *J. Climate*, 26(8), 2546-2556, <https://doi.org/10.1175/JCLI-D-12-00062.1>, 2013

623 Clementi, E., Oddo, P., Drudi, M., Pinardi, N., Korres, G., and Grandi A. Coupling hydrodynamic and wave models: first step
624 and sensitivity experiments in the Mediterranean Sea. *Ocean Dynam.*, 67(10), 1293-1312, [https://doi.org/10.1007/s10236-](https://doi.org/10.1007/s10236-017-1087-7)
625 [017-1087-7](https://doi.org/10.1007/s10236-017-1087-7), 2017

626 Clementi, E., Aydogdu, A., Goglio, A. C., Pistoia, J., Escudier, R., Drudi, M., Grandi, A., Mariani, A., Lyubartsev, V., Lecci,
627 R., Cretí, S., Coppini, G., Masina, S., & Pinardi, N.. Mediterranean Sea Physical Analysis and Forecast (CMEMS MED-
628 Currents, EAS6 system) (Version 1) [[Data set](#)]. Copernicus Monitoring Environment Marine Service (CMEMS), 2021. Deser,
629 C., Alexander, M. A., Xie, S. P., and Phillips, A. S., Sea surface temperature variability: Patterns and mechanisms. *Annu. Rev.*
630 *Mar. Sci.* 2, 115-143, <https://doi.org/10.1146/annurev-marine-120408-151453>, 2010

631 Dobricic, S., and Pinardi, N.. An oceanographic three-dimensional variational data assimilation scheme. *Ocean Model.*, 22(3-
632 4), 89-105, <https://doi.org/10.1016/j.ocemod.2008.01.004>, 2008

633 Efron, B.; Tibshirani, R.J. *An Introduction to the Bootstrap*; CRC Press: Boca Raton, FL, USA, 1994.

634 Fiedler, E. K., McLaren, A., Banzon, V., Brasnett, B., Ishizaki, S., Kennedy, J., ... and Donlon, C. Intercomparison of long-
635 term sea surface temperature analyses using the GHRSSST Multi-Product Ensemble (GMPE) system. *Remote Sens. Environ.*,
636 222, 18-33, <https://doi.org/10.1016/j.rse.2018.12.015>, 2019

637 Gentemann, C. L. Minnett, P. J., Le Borgne, P., and Merchant, C. J. Multi-satellite measurements of large diurnal warming
638 events. *Geophysical Research Letters*, 35 (22), L22602. <http://dx.doi.org/10.1029/2008GL035730>,
639 <https://doi.org/10.1029/2008GL035730>, 2008

640 Good, S. A., Corlett, G. K., Remedios, J. J., Noyes, E. J., and Llewellyn-Jones, D. T.. The global trend in sea surface
641 temperature from 20 years of advanced very high resolution radiometer data. *J. Climate*, 20(7), 1255-1264,
642 <https://doi.org/10.1175/JCLI4049.1>, 2007

643 Good, S., Fiedler, E., Mao, C., Martin, M.J., Maycock, A., Reid, R., Roberts-Jones,
644 J., Searle, T., Waters, J., While, J., and Worsfold, M.. The Current Configuration of the OSTIA System for Operational
645 Production of Foundation Sea Surface Temperature and Ice Concentration Analyses. *Remote Sens.-BASEL*, 12(4),720,
<https://doi.org/10.3390/rs12040720>, 2020.

646 Huang, B., Liu, C., Freeman, E., Graham, G., Smith, T., & Zhang, H. M.. Assessment and Intercomparison of NOAA Daily
647 Optimum Interpolation Sea Surface Temperature (DOISST) Version 2.1. *J. Climate*, 34(18), 7421-7441.

648 Kotsias, G., & Lolis, C. J.. A study on the total cloud cover variability over the Mediterranean region during the period 1979–
649 2014 with the use of the ERA-Interim database. *Theor. Appl. Climatol.*, 134(1), 325-336, [https://doi.org/10.1175/JCLI-D-21-](https://doi.org/10.1175/JCLI-D-21-0001.1)
650 [0001.1](https://doi.org/10.1175/JCLI-D-21-0001.1), 2018

651 Le Traon, P. Y., Reppucci, A., Alvarez Fanjul, E., Aouf, L., Behrens, A., Belmonte, M., ... and Zacharioudaki, A. From
652 observation to information and users: The Copernicus Marine Service perspective. *Frontiers in Marine Science*, 6, 234,
653 <https://doi.org/10.3389/fmars.2019.00234>, 2019.

654 Marullo, S., Minnett, P. J., Santoleri, R., and Tonani, M.. The diurnal cycle of sea-surface temperature and estimation of the
655 heat budget of the Mediterranean Sea. *J.Geophys.Res.-Oceans*, 121(11), 8351-8367, <https://doi.org/10.1002/2016JC012192>,
656 2016

657 Marullo, S., Santoleri, R., Ciani, D., Le Borgne, P., Péré, S., Pinardi, N., Tonani, M., and Nardone, G.. Combining model
658 and geostationary satellite data to reconstruct hourly SST field over the Mediterranean Sea. *Remote Sens. Environ.*, 146, 11-
23, <https://doi.org/10.1016/j.rse.2013.11.001>, 2014

659 Merchant, C. J., Embury, O., Bulgin, C. E., Block, T., Corlett, G. K., Fiedler, E., ... and Donlon, C.. Satellite-based time-series
660 of sea-surface temperature since 1981 for climate applications. *Scientific data*, 6(1), 1-18, 2019.

661 Merchant, C. J., Filipiak, M. J., Le Borgne, P., Roquet, H., Autret, E., Piollé, J. F., & Lavender, S. . Diurnal warm-layer events
662 in the western Mediterranean and European shelf seas. *Geophys. Res. Lett.*, 35(4), <https://doi.org/10.1029/2007GL033071>,
663 2008

664 Minnett, P. J., Alvera-Azcárate, A., Chin, T. M., Corlett, G. K., Gentemann, C. L., Karagali, I., ... and Vazquez-Cuervo, J. .
665 Half a century of satellite remote sensing of sea-surface temperature. *Remote Sens. Environ.*, 233, 111366,
666 <https://doi.org/10.1016/j.rse.2019.111366>, 2019

667 Oddo, P., Adani, M., Pinardi, N., Fratianni, C., Tonani, M., and Pettenuzzo, D. A Nested Atlantic-Mediterranean Sea General
668 Circulation Model for Operational Forecasting. *Ocean Sci. Discuss.*, 5(4), 461-473, <https://doi.org/10.5194/os-5-461-2009>,
669 2009.

670 Oddo, P., Bonaduce, A., Pinardi, N., and Guarneri, A. Sensitivity of the Mediterranean sea level to atmospheric pressure and
671 free surface elevation numerical formulation in NEMO. *Geosci. Model Dev.*, 7, 3001–3015, [https://doi.org/10.5194/gmd-7-
672 3001-2014](https://doi.org/10.5194/gmd-7-3001-2014), 2014.

673 Oliver, E. C., Benthuisen, J. A., Darmaraki, S., Donat, M. G., Hobday, A. J., Holbrook, N. J., ... and Sen Gupta, A. . Marine
674 heatwaves. *Annu. Rev. Mar. Sci.*, 13, 313-342, <https://doi.org/10.1146/annurev-marine-032720-095144>, 2021 Pinardi, N.,
675 Allen, I., De Mey, P., Korres, G., Lascaratos, A., Le Traon, P.Y., Maillard, C., Manzella G., and Tziavos, C. . The
676 Mediterranean ocean Forecasting System: first phase of implementation (1998-2001). *Ann. Geophys.*, 21, 1, 3-20,
677 <https://doi.org/10.5194/angeo-21-3-2003>, 2003.

678 Pisano, A., Marullo, S., Artale, V., Falcini, F., Yang, C., Leonelli, F. E., ... and Buongiorno Nardelli, B.. New evidence of
679 mediterranean climate change and variability from sea surface temperature observations. *Remote Sens.-BASEL*, 12(1), 132,
680 <https://doi.org/10.3390/rs12010132>, 2020

681 Pisano, A., Buongiorno Nardelli, B., Marullo, S., Rosalia, S., Tronconi, C., & Ciani, D. (2021). Mediterranean Sea - High
682 Resolution Diurnal Subskin Sea Surface Temperature Analysis (Version 1) [Data set]. Copernicus Marine Environment
683 Monitoring Service (CMEMS). https://doi.org/10.25423/CMCC/SST_MED_PHY_SUBSKIN_L4_NRT_010_036

684 Pisano, Andrea. (2021). CNR Mediterranean Sea High Resolution Diurnal Subskin Sea Surface Temperature Analysis:
685 Validation subset. <https://doi.org/10.5281/zenodo.5807729>

686 Reverdin, G., Boutin, J., Martin, N., Lourenço, A., Bouruet-Aubertot, P., Lavin, A., ... and Lazure, P.. Temperature
687 measurements from surface drifters. *J. Atmos. Ocean.Tech.* 27(8), 1403-1409, <https://doi.org/10.1175/2010JTECHO741.1>,
688 2010.

689 Rio, M. H., and Santoleri, R.. Improved global surface currents from the merging of altimetry and sea surface temperature
690 data. *Remote Sens. Environ.*, 216, 770-785, <https://doi.org/10.1016/j.rse.2018.06.003>, 2018

691 Storto, A., and Oddo, P. . Optimal assimilation of daytime SST retrievals from SEVIRI in a regional ocean prediction system.
692 *Remote Sens.-BASEL*, 11(23), 2776, <https://doi.org/10.3390/rs11232776>, 2019

693 Takaya, Y., Bidlot, J. R., Beljaars, A. C., & Janssen, P. A.. Refinements to a prognostic scheme of skin sea surface temperature.
694 *J Geophys. Res-Oceans*, 115(C6), <https://doi.org/10.1029/2009JC005985>, 2010

695 Yang, C., Leonelli, F. E., Marullo, S., Artale, V., Beggs, H., Nardelli, B. B., ... and Pisano, A.. Sea Surface Temperature
696 Intercomparison in the Framework of the Copernicus Climate Change Service (C3S). *J. Climate*, 34(13), 5257-5283,
697 <https://doi.org/10.1175/JCLI-D-20-0793.1>, 2021

698 Waters, J., Lea, D. J., Martin, M. J., Mirouze, I., Weaver, A., and While, J.. Implementing a variational data assimilation
699 system in an operational 1/4 degree global ocean model. *Q. J. Roy. Meteor. Soc.*, 141(687), 333-349,
700 <https://doi.org/10.1002/qj.2388>, 2015

701 While, J., Mao, C., Martin, M. J., Roberts-Jones, J., Sykes, P. A., Good, S. A., and McLaren, A. J.. An operational analysis
702 system for the global diurnal cycle of sea surface temperature: implementation and validation. *Q. J. Roy. Meteor. Soc.*,
703 143(705), 1787-1803, <https://doi.org/10.1002/qj.3036>, 2017. Zeng, X., Zhao, M., Dickinson, R. E., & He, Y.. A multi-year
704 hourly sea surface skin temperature dataset derived from the TOGA TAO bulk temperature and wind speed over the tropical
705 Pacific. *J. Geophys. Res-Oceans*, 104, 1525–1536, <https://doi.org/10.1029/1998JC900060>, 1999

706 Zeng, X., Zhao, M., Dickinson, R. E., & He, Y. (1999). A multi-year hourly sea surface skin temperature dataset derived from
707 the TOGA TAO bulk temperature and wind speed over the tropical Pacific. *J. of Geophysical Res.*, 104, 1525–1536.

708

709

710



711

712